Nanoscale

PAPER

View Article Online
View Journal

Cite this: DOI: 10.1039/c7nr00886d

Bio-inspired, colorful, flexible, defrostable light-scattering hybrid films for the effective distribution of LED light†

Seongpil An,‡[a] Hong Seok Jo,‡[a] Yong Il Kim,[a] Kyo Yong Song,[a] Min-Woo Kim,[a] Kyu Bum Lee,[b] Alexander L. Yarin *[a,c] and Sam S. Yoon *[a]

Received 9th February 2017,
Accepted 3rd June 2017

DOI: 10.1039/c7nr00886d

rsc.li/nanoscale

Bioluminescent jellyfish has a unique structure derived from fiber/polymer interfaces that is advantageous for effective light scattering in the dark, deep sea water. Herein, we demonstrate the fabrication of bio-inspired hybrid films by mimicry of the jellyfish's structure, leading to excellent light-scattering performance and defrosting capability. A haze value reaching 59.3% and a heating temperature of up to 292 °C were achieved with the films. Accordingly, the developed surface constitutes an attractive optical device for lighting applications, especially for street or vehicle luminaries for freezing Arctic-climate countries. The morphological details of the hybrid films were revealed by scanning electron microscopy. The light-scattering properties of these films were examined by ultraviolet-visible-infrared spectrophotometry and anti-glare effect analyses. The defrosting performance of the hybrid films was evaluated *via* heating tests and infra-red observations.

1. Introduction

Light-emitting diodes (LEDs), which are considered as one of the most efficient lighting sources,[1] have become an essential everyday material. LEDs are commonly used in indoor bulbs in buildings,[2] outdoor lights on the streets, and various lamps for vehicles, portable devices, and even fishing boats.[3] According to the U.S. Government report,[4] the electricity consumed for lighting applications in the United States accounts for 22% of the total electricity generated. With the explosion of global industrialization and population in recent decades, the demand for LED lighting systems has risen sharply, thereby fueling intensive research and development efforts related to LED technology. Accordingly, the LED performance, indicated by the efficiency, lifetime, response time, and durability, has undergone remarkable improvement.[5]

However, despite such improvements, the use of LEDs as a luminary has faced ongoing challenges due to the non-uniform light distribution of current LEDs, which causes a glare effect on human eyes as well as non-compliance in many lighting applications.[3,6–9] Hitherto, various approaches have been attempted to achieve an anti-glare effect, especially to prevent eye damage and to address the concerns related to lighting applications. An addendum optical device, called a secondary lens or a freeform surface, has been developed, and it has been applied to practical LED luminaries.[3,7,10] These additional lenses are designed to re-distribute the light from LEDs to achieve glare reduction and light uniformity. However, the demand for device miniaturization (*i.e.*, weight and size reduction) for industrial purposes requires the development of miniature lenses for micro-devices, which is hampered by the design limits and the corresponding high-cost of mass production.

In addition, in the freezing Arctic-climate countries, such as the US, Canada, Greenland, and Russia, and even in non-Arctic-climate countries during the winter season, degradation of the performance of LEDs due to frost has been a significant problem with attendant economic losses and safety problems. To overcome this issue, a novel, practical method for application of LED luminaries should be proposed and developed to effectively harness the lucrative luminary market.

Recently, Lee *et al.*[11] introduced a novel composite thin layer composed of electrospun polyacrylonitrile (PAN) nanofibers (NFs) and the SU-8 polymer. The electrospun polymer NFs in the composite layer could efficiently distribute LED light due to the light-scattering phenomenon resulting from the fiber/polymer interfaces.[12] To better characterize the light

[a]*School of Mechanical Engineering, Korea University, Seoul 02841, Republic of Korea. E-mail: skyoon@korea.ac.kr*
[b]*NGL Co. Ltd, Gyeonggi-do 15843, Republic of Korea*
[c]*Department of Mechanical and Industrial Engineering, University of Illinois at Chicago, 842 W. Taylor St., Chicago, IL 60607-7022, USA. E-mail: ayarin@uic.edu*
†Electronic supplementary information (ESI) available. See DOI: 10.1039/c7nr00886d
‡These authors contributed equally to this work.

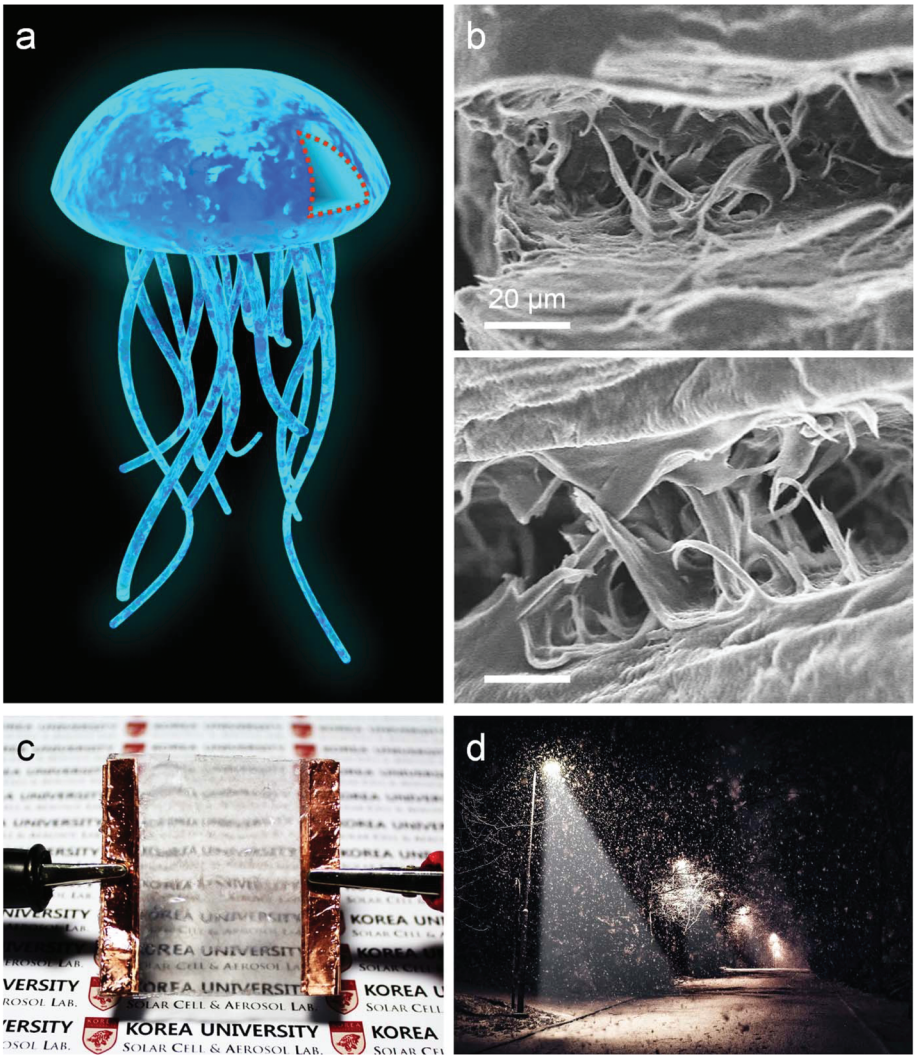

Fig. 1 (a) Schematic of a bioluminescent jellyfish. (b) SEM images of the jellyfish body. (c) Photograph of the flexible hybrid film (*cf.* Fig. 7d). (d) Artistic rendition of a street on a snowy day where the hybrid film-treated LED luminaries are installed.

distribution effect and thus to achieve the anti-glare effect, the authors studied the effects of the NF diameter and content on the optical properties of the composite. More recently, it was found that light-scattering capabilities are demonstrated by various bioluminescent marine organisms, where light-scattering is employed for luring food, attracting mates, and threatening enemies.[13] In particular, jellyfish possesses a structure reminiscent of the aforementioned fiber/polymer interfaces, which is called a mesogloea and is located in the gelatinous umbrella-shaped jellyfish body as shown in Fig. 1a, b and S1.†[14]

Herein, a hybrid film (Fig. 1c) is fabricated to achieve light distribution as well as defrosting effects. The hybrid film exhibits an excellent light-scattering and defrosting performance without any significant loss of the luminous flux. The hybrid film is multi-layered and composed of a polymer NF-embedded composite and a transparent metal microfiber (MF) layer. The developed film holds great promise as a lucrative luminary for application on streets, in buildings, in military devices, *etc.* (Fig. 1d).

2. Experimental section

2.1. Electrospinning nanofibers

Polyacrylonitrile (PAN, M_w = 150 kDa, Sigma-Aldrich) and *N*,*N*-dimethylformamide (DMF, 99.8%, Sigma-Aldrich) were used as the solute and solvent, respectively, to prepare the electrospinning solution. 10 wt% PAN powder was dissolved in DMF solution and magnetically stirred for 24 h at room temperature. Electrospinning was conducted using a setup composed of a syringe pump (Legato 100, KD Scientific) and a DC power supply (EL20P2, Glassman High Voltage, Incorporated). The electrospinning flow rate was 300 μL h^{-1} and the applied high DC voltage was 8 kV. The electrospinning time (t_1) was set at 5, 15, 30, 60, or 120 min to compare the light-scattering effects

with variation of the nanofiber (NF) layer thickness and porosity. An 18-gauge needle (Nordson EFD) installed in the syringe pump was used and the needle-to-substrate distance was 15 cm.

2.2. Cu-microfibers

8 wt% PAN solution was electrospun onto a Cu-frame for the fixed electrospinning time (t_1) of 2 s at a flow rate of 300 μL h^{-1} using a high DC voltage of 8 kV. An 18-gauge needle (Nordson EFD) was used, and the needle-to-substrate distance was 15 cm. Prior to electroplating, Pt seeds were sputtered onto the PAN NFs to facilitate electroplating of the NFs. In addition, a second layer of PAN NFs (which were not Pt-sputtered) was subsequently electrospun onto the Cu-frame for 2 min to mechanically support the first electrospun layer of NFs (which were Pt-sputtered) in the electroplating process. The Cu-frame was then electroplated with Cu for 7 s at an applied voltage of 3 V, and accordingly, only the Pt-sputtered NFs were electroplated. The Cu-electroplated sample was then rinsed with DI water and 10% formaldehyde. The rinsed sample was dried under a nitrogen atmosphere for a few hours to prevent oxidation. Finally, the sample was rinsed again with DMF solution to remove the second layer of electrospun NFs. The details of the electroplating process and materials are described in ref. 15 and 16. Note that the second layer of PAN NFs was not removed in the case of a single-layered hybrid film.

2.3. Characterization

A jellyfish body, the PAN NFs, and the Cu-microfibers (CuMFs) were analyzed by field-emission scanning electron microscopy (FE-SEM, S-5000, Hitachi). The jellyfish was purchased from the market. The average fiber diameters were determined by measuring 200 NFs from the SEM images (*cf.* Fig. 2) by using imaging software (I'MEASURE, INGPLUS). The parallel transmittances, T_r, in Fig. 3 were obtained by using an ultraviolet-visible spectrophotometer (Optizen POP, Mecasys), where T_r is based on the glass (T_r = 100%) and varies at different wavelengths (λ). Note that heat-resistant glass (D263) was used for all of the films. The total, parallel, and diffuse transmittances, and the haze values in Table 1 were obtained by the ASTM standard test method D1003 with a haze meter (HM-150, Murakami) that was examined by the governing office of the Korea Polymer Testing & Research Institute (KOPTRI, Seoul, Republic of Korea). Note that the parallel transmittance values in Fig. 3 and Table 1 differ slightly (by about 2–7%) because different devices were used. A few droplets of inner inks in oil-based markers purchased from the market were used to dye the PAN solution in Fig. 4. The steady-state temperature of the hybrid film surface was measured by using a thermocouple and a data recorder (MV1000, Yokogawa). The luminous flux, the luminescence efficiency, and the Commission Internationale de I'Eclairage (CIE) chromaticity coordinates were measured by using an ultraviolet-visible-infrared spectrophotometer (PMS-80, EVERFINE) that was examined by the

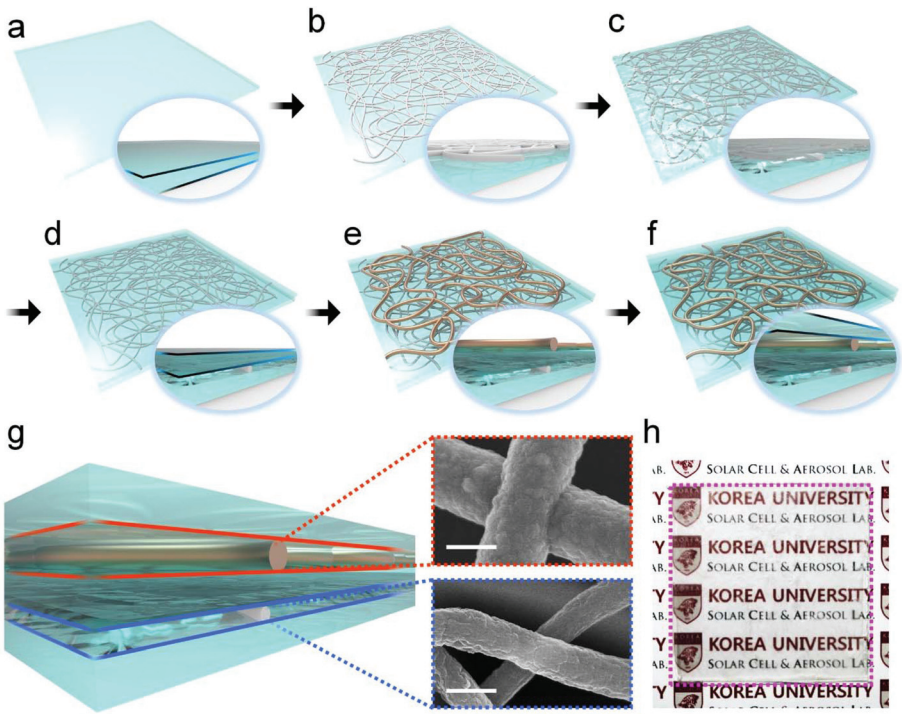

Fig. 2 Schematics of the process of fabrication of the hybrid film. (a) Bare bottom glass. (b) PAN NFs deposited on the glass. (c) PDMS was poured onto the NFs. (d) The middle glass was placed on the NF/PDMS composite. (e) Cu-microfibers (CuMFs) were transferred onto the middle glass. (f) The top glass was placed on the CuMFs. (g) Cross-sectional schematic view of the hybrid film. SEM images of the CuMFs (red-marked) and PAN NFs (blue-marked). The inset scale bars are 1 μm. (h) Photograph of the hybrid film for t_1 = 120 min.

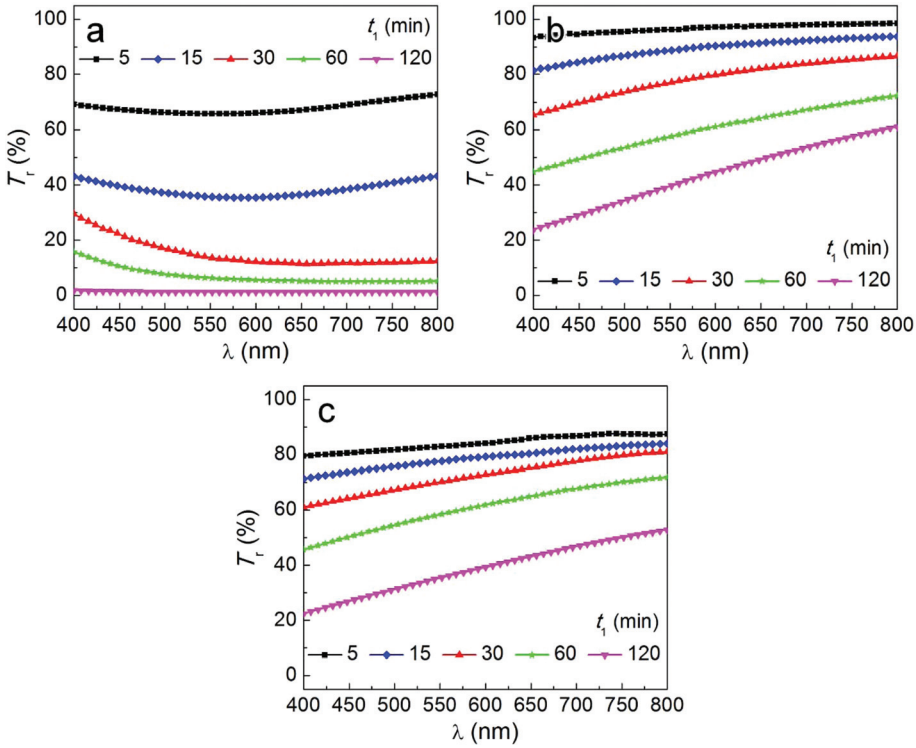

Fig. 3 Parallel transmittance, T_r, *versus* the wavelength of light, λ, after each fabrication process. (a) Light-scattering layers (on the glass) before applying PDMS (*cf.* Fig. 2b). (b) Light-scattering layers (on the glass) after applying PDMS and the middle glass (*cf.* Fig. 2d). (c) The hybrid films (where the defrosting layers and the top glasses were applied, *cf.* Fig. 2f).

Table 1 Transmittance and haze values of the hybrid films for different values of t_1

t_1 (min)	Total transmittance (T_t, %)	Parallel transmittance (T_r, %)	Diffuse transmittance (T_d, %)	Haze (%)
0 (bare glass)	91.6	91.5	0.1	0.11
5	91.3	86.5	4.8	5.30
15	92.1	81.0	11.1	12.1
30	90.9	75.5	15.4	16.9
60	90.1	54.0	36.1	40.1
120	87.6	35.7	51.9	59.3

lighting company, NGL (Gyeonggi-do, Republic of Korea). A white SMD LED lamp (LEMWS36X, LG Innotek) was used for all lighting experiments.

3. Results and discussion

3.1. Hybrid film

Lee *et al.*[11] studied the effects of the diameter and the amount of PAN NFs on the optical characteristics and the corresponding anti-glare effects of the light-scattering layers. The 10 wt% PAN NF sample prepared by using an electrospinning time of t_1 = 10 min gave rise to the highest light distribution performance among the evaluated samples. In the present study, a single electrospinning solution with a concentration of 10 wt% was used to fabricate the light-scattering layer and the first electrospinning time, t_1, was varied from 5 to 120 min, which is wider than the range previously utilized. Fig. 2a–d illustrate the fabrication process for the light-scattering layer. The 10 wt% PAN solution was deposited onto a bare (or bottom) glass by electrospinning (see Fig. 2a, b, and section 2.1). A moderate amount of PDMS was then poured onto the NF-coated glass (Fig. 2c) and a second (or middle) glass was subsequently placed on the wet NF/PDMS composite and left until fully dried (Fig. 2d). It should be emphasized that a different size glass (5 × 5 cm^2, Fig. S2†) was used in this study compared to that used in the previous study (3 × 3 cm^2), which resulted in different transmittances even when t_1 was the same. Fig. S2a and S3† show the photographs and SEM images of the PAN NFs on the glass before applying PDMS for different values of t_1. Non-woven, uniformly deposited PAN NFs were observed in all cases. No discernible difference was observed as t_1 increased. The average fiber diameters were 492 ± 99, 528 ± 117, 553 ± 94, 522 ± 87, and 633 ± 115 nm at t_1 = 5, 15, 30, 60, and 120 min, respectively (Fig. S4†). These both average diameters are over 400 nm and the fibrous structure (*cf.* Fig. S3†) facilitated the effective light-scattering effect of the hybrid films as discussed in ref. 12, section 3.2 and illustrated in Fig. S5.† The incident light is reflected or refracted due to the differences of the reflective indexes between different materials, which is considerable especially

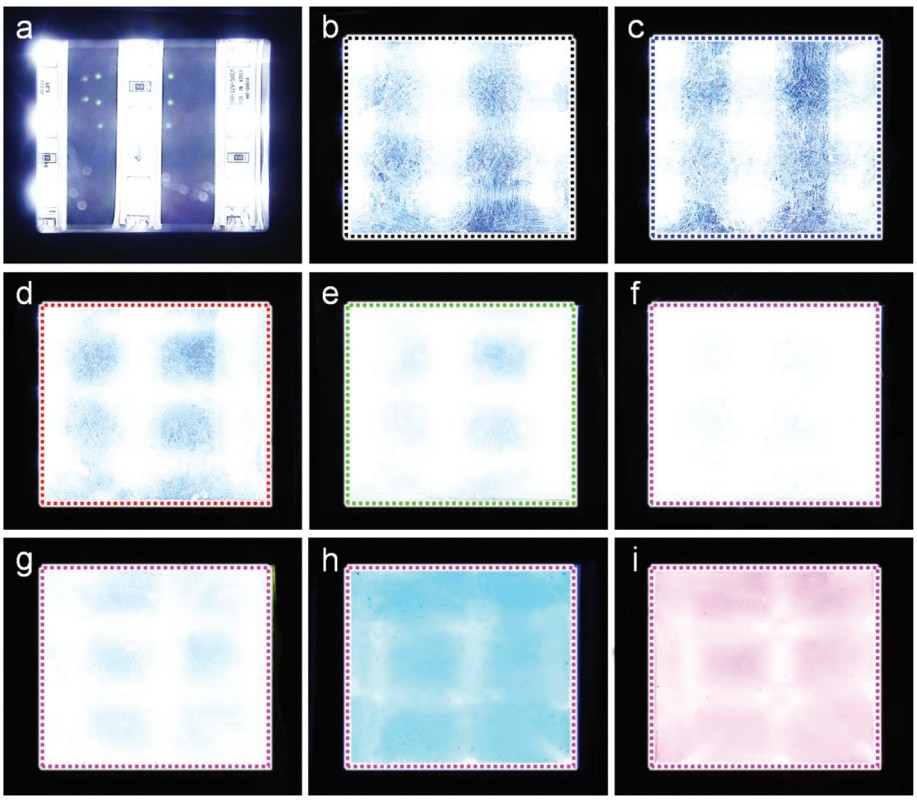

Fig. 4 Anti-glare effect of the hybrid films as a function of the first electrospinning time, t_1: (a) bare glass, (b) t_1 = 5 min, (c) t_1 = 15 min, (d) t_1 = 30 min, (e) t_1 = 60 min, and (f) t_1 = 120 min. The anti-glare effects of the colored hybrid films electrospun for t_1 = 120 min (g) Yellow. (h) Blue. (i) Red.

at the fiber/polymer interfaces (*cf.* Fig. S5†), thereby causing the light-scattering phenomenon.

The transparent defrosting layer was composed of Cu-microfibers (CuMFs). The CuMFs were prepared by a method similar to that described in detail in our previous study (*cf.* section 2.2).[16] The following process for fabrication of the defrostable light-scattering hybrid film is illustrated in Fig. 2e and f. The prepared transparent defrosting layer was transferred onto the light-scattering layer as illustrated in the cross-sectional schematic in Fig. 2e. A third (or top) glass was then placed on the defrosting layer (Fig. 2f). Note that PDMS was pasted onto the sides to seal the entire film.

Fig. 3 shows the changes in the parallel transmittance (T_r) *versus* the light wavelength (λ) during progress of the fabrication process. Before applying PDMS to the light-scattering layers (*cf.* Fig. 2b and S1a†), T_r decreased from 66% to 1% (at λ = 550 nm) as the value of t_l increased from 5 to 120 min (Fig. 3a). After applying PDMS and the middle glass (*cf.* Fig. 2d and S1b†), in all cases, T_r increased by about 30–50% (Fig. 3b) due to the reduction of the reflection coefficient as described in detail elsewhere.[17] Fig. 3c shows a plot of T_r *versus* λ for the finally-fabricated hybrid films (*cf.* Fig. 2f and S1c†). After applying the transparent defrosting layer (*cf.* Fig. 2f), the overall T_r values decreased slightly (by 10%). Note that for the transparent defrosting layer, $T_r \sim 90\%$. Even though T_r decreased with the application of the defrosting layer, it should be emphasized that the total transmittance (T_t) remained as high as $T_t \sim 90\%$ (Table 1). Note also that T_t comprises T_r and the diffuse transmittance (T_d), as illustrated in Fig. S6.†[18] Although T_r decreased from 86.5% to 35.7%, T_d increased from 4.8% to 51.9% without any significant change in the value of T_t as t_1 increased (Table 1), which resulted in a dramatic increase of the haze value from 5.3% to 59.3%, where the haze is defined as follows: haze = $(T_d/T_t) \times 100$. Due to the haze effect, the anti-glare effect due to the light distribution was enhanced as described in section 3.2.

3.2. Light-scattering performance of the hybrid film

To compare the overall anti-glare effect of the hybrid films as a function of the first electrospinning time, anti-glare tests were performed as shown in Fig. 4. The tests were conducted in a dark room and nine LED lamps were placed at the bottom of the setup (*cf.* Fig. 4a). The film-to-bottom distance was 5 cm. With an increase of t_1 from t_1 = 0 to t_1 = 120 min (Fig. 4a–f), a complete anti-glare effect was achieved at t_1 = 120 min, whereas the glare was still apparent up to t_1 = 30 min. It should be emphasized that a perfect anti-glare effect was achieved at t_1 = 120 min in conjunction with a high luminous flux (f_l) of f_l = 320 lm and a high luminescence efficiency (η_l) of η_l = 29.6 lm W^{-1}, the values of which were 90% of those of the bare glass substrate (Table 2). Fig. 4g–i and Fig. S7† show the anti-glare effects of the colored hybrid films at t_1 = 120 min. These films were fabricated by electrospinning the

Table 2 Parameters of the hybrid film-applied LED luminaries for different values of the first electrospinning time t_1

t_1 (min)	Luminous flux (f_l, lm)	Luminescence efficiency (η_l, lm W^{-1})	CIE coordinates	
			x	y
0 (bare glass)	360	33.4	0.3414	0.3486
5	355	32.9	0.3412	0.3490
15	350	32.5	0.3409	0.3493
30	349	32.4	0.3411	0.3486
60	347	32.3	0.3411	0.3490
120	320	29.7	0.3419	0.3494

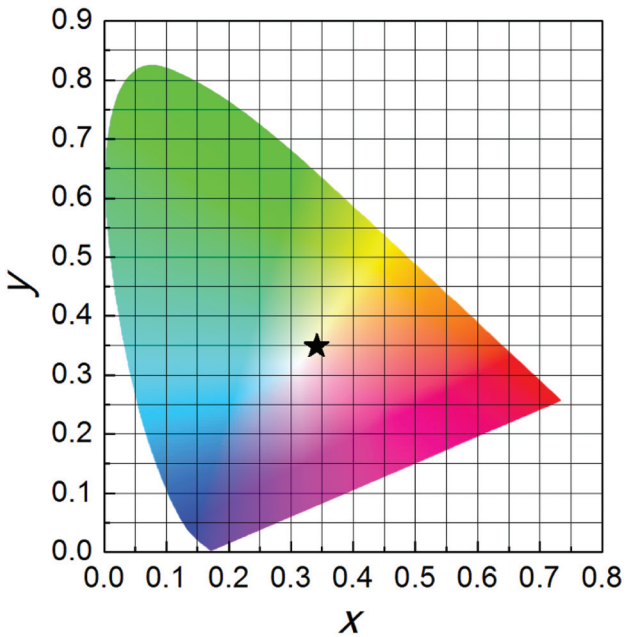

Fig. 5 CIE 1931 color coordinates of the hybrid films.

dyed PAN solution. The light-scattering layer can be easily treated with almost any color without using active materials or color filters, which should be economically advantageous for many luminaries. In addition, even though a patterned hybrid film is not shown here, it is possible to weave or pattern nanofibers as shown in the previous studies,[19–21] which further facilitates the possibility of using such hybrid films in microdevices.

Fig. 5 shows the Commission Internationale de I'Eclairage (CIE) 1931 color coordinates of the hybrid films. As listed in Table 2, the x and y values of the hybrid films, respectively, varied by 0.0005 and 0.0008 with the variation of t_1, compared to the values for the bare glass. Accordingly, the percentage variation in the x and y values were 0.15% and 0.23%, respectively, indicating that there were no light distortion effects due to light scattering and defrosting layers.

3.3. Heating performance of the hybrid film

Recently, transparent thin heaters composed of one-dimensional electrical materials such as carbon nanotubes (CNTs)[22,23] and silver nanowires (AgNWs)[24,25] have gained prominence as they hold great promise for various engineering applications, including smart windows, solar panels, home appliances, and so on.[26,27] Similar one-dimensional metal wires are known to be among the most attractive materials as they demonstrate both high transparency and high electrical conductivity. Accordingly, highly transparent conductive Cu-microfibers (CuMFs) are also attractive for transparent thin heaters. Fig. 6a illustrates the heating performance of such hybrid films as a function of time and applied voltage (V_a). Note that the heating performance was not related to t_1 for the light-scattering layer because identical CuMFs were used in all cases. The steady-state temperature (T) was measured with stepwise increases in V_a. The temperature increased from room temperature (23 °C) to 292 °C as the value of V_a increased from 0 to 3.5 V. Even though the CuMFs were broken above V_a = 3.5 V at T = 292 °C, it should be emphasized that below T = 292 °C the material is effective enough to melt snow even under extremely freezing conditions. Fig. 6b illustrates the thermal stability and durability of the hybrid film for 22 cycles at V_a = 2.5 V. The peak values of T were invariable over 22 cycles, which reveals the possibility for practical use of such heaters in lighting applications. Note that the step-wise increase in V_a (Fig. 6a) resulted in a higher temperature (50 °C) compared to the case where V_a was constant (Fig. 6b) even at the same value of V_a, probably due to the transient character of the process.

Fig. 6c and Movie S1† illustrate the results of the defrosting test with the hybrid film. The test conditions were set to mimic the frost and snowing problems in freezing climates, especially for outdoor lighting applications. To reveal the defrosting capability in the case of a thick snow layer, an ice-stacked duct was used, as shown in Fig. 6c. Gradual melting of the ice was observed when the voltage applied to the film was V_a = 3.2 V. Melting of the ice layer began immediately and was completed within 225 s. Note that the surface temperature of the hybrid film was $T \sim 200$ °C and water resulting from the melting ice flowed through the hole located at the bottom of the duct. The defrosting performance in the case of the thick ice layer demonstrates unequivocally that the hybrid film holds potential for specific lighting applications under freezing climatic conditions.

3.4. Single-layered and flexible hybrid films

Even though a multi-layered structure such as the hybrid film shown in Fig. 2f is the most appropriate means of preventing degradation of the PAN nanofibers by the high temperature of the defrosting layer, it should be emphasized that a single-layered hybrid film could also be fabricated as shown in Fig. 7a and b. The second layer of the electrospun PAN NFs discussed in section 2.2 can play the role of a light-scattering layer if the NFs from the second layer are not removed by dissolution in DMF. Note that the T_r value of the single-layered hybrid film in Fig. 7a was 93%. That is, it is unnecessary to include a separate light-scattering layer in the single-layered

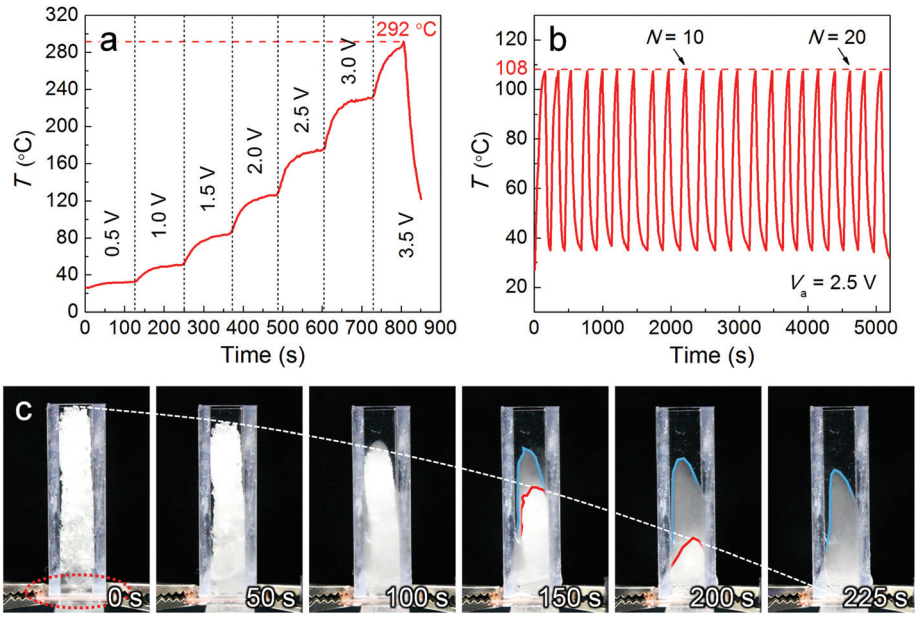

Fig. 6 Heating and defrosting performance of the hybrid film. (a) Temperature *versus* time plot. (b) Thermal stability test with on/off power switching for 20 cycles at V_a = 2.5 V. (c) Photographs taken during defrosting test with the hybrid film at V_a = 3.2 V at different times. The white-dashed line indicates the height of the ice layer. The red-dashed circle indicates the location of the hybrid film. The blue and red straight lines indicate the vapor adhering to the wall and the ice, respectively.

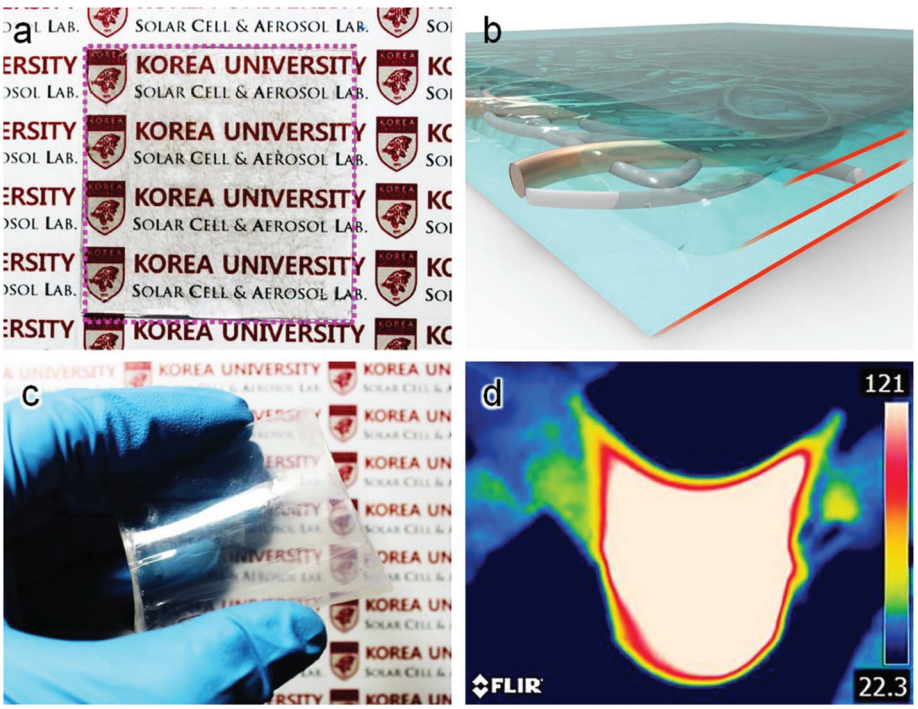

Fig. 7 (a) Photograph and (b) schematic illustration of the single-layered film. (c) Photograph and (d) infrared image of the flexible hybrid film (t_1 = 120 min, V_a = 2.5 V).

hybrid film, particularly for application under low temperature conditions.

Furthermore, it should be emphasized that both the multi-layered and the single-layered hybrid films can be fabricated in a flexible form, as depicted in Fig. 7c and d. Indeed, replacing the glasses with flexible PET films conferred flexibility to the hybrid film. Both the multi-layered and the single-layered hybrid films showed impressive results in the bending cycle

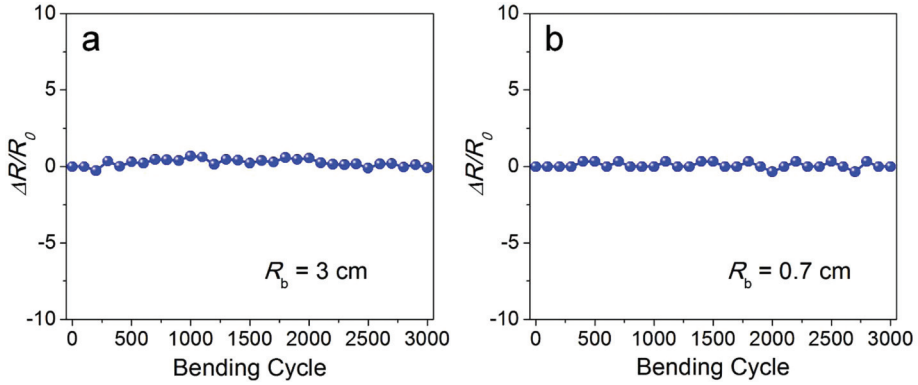

Fig. 8 Bending cycle tests of (a) the flexible multi-layered (t_1 = 120 min) and (b) the flexible single-layered hybrid films.

tests, as shown in Fig. 8a and b. During 3000 cycles, both films retained their electrical conductivities that means there was no significant degradation affecting the heating. Note also that both the multi-layered and the single-layered hybrid films maintained their conductivities almost constant as the bending radius decreased to 9 and 1 mm, respectively. These results unequivocally demonstrate another avenue for producing next-generation micro-devices.

4. Conclusions

Multi-layered, bio-inspired hybrid films that possess light-scattering capabilities were successfully developed. The films were transparent, and they could be heated by an electric current for use as defrosting layers. These bio-inspired films were formed in a two-step process *via* electrospinning followed by electroplating. The light-scattering layers are composed of non-woven electrospun PAN nanofibers embedded in a PDMS matrix, which facilitates efficient light distribution with a high haze value of up to 59.3%. This high haze value is attributed to the fiber/polymer interfaces that closely emulate the mesogloea morphology of the gelatinous umbrella-shaped jellyfish body. The transparent defrosting layers are formed from a network of conducting Cu-electroplated polymer nanofibers. The Cu-electroplated fibers in the hybrid film contribute to the superior defrosting performance, resulting in a heating temperature of up to 292 °C when a low voltage of 3.5 V is applied. In addition, the hybrid films undergo color changes and exhibit mechanical flexibility. These bio-inspired films hold great promise for various luminary applications.

Acknowledgements

This research was supported by the Technology Development Program to Solve Climate Changes of the National Research Foundation (NRF) funded by the Ministry of Science, ICT & Future Planning (2016M1A2A2936760) and NRF-2017R1A2B4005639. This work was also supported by the National Research Council of Science & Technology (NST) grant by the Korea government (MSIP) (no. CRC-16-02-KICT).

References

1 S. Pimputkar, J. S. Speck, S. P. DenBaars and S. Nakamura, *Nat. Photonics*, 2009, **3**, 180–182.
2 B.-L. Ahn, C.-Y. Jang, S.-B. Leigh, S. Yoo and H. Jeong, *Appl. Energy*, 2014, **113**, 1484–1489.
3 M.-F. Lai, N. D. Q. Anh, J.-Z. Gao, H.-Y. Ma and H.-Y. Lee, *Appl. Opt.*, 2015, **54**, E69–E74.
4 U. D. o. E. S.-S. L. R. a. Development, *Multi-Year Program Plan FY'09-FY'14*.
5 M.-H. Chang, D. Das, P. Varde and M. Pecht, *Microelectron. Reliab.*, 2012, **52**, 762–782.
6 F. Behar-Cohen, C. Martinsons, F. Viénot, G. Zissis, A. Barlier-Salsi, J. Cesarini, O. Enouf, M. Garcia, S. Picaud and D. Attia, *Prog. Retinal Eye Res.*, 2011, **30**, 239–257.
7 R. Hu, X. Luo, H. Zheng, Z. Qin, Z. Gan, B. Wu and S. Liu, *Opt. Express*, 2012, **20**, 13727–13737.
8 X.-H. Lee, I. Moreno and C.-C. Sun, *Opt. Express*, 2013, **21**, 10612–10621.
9 I. Ullah and S. Shin, *Energy Build.*, 2014, **72**, 246–261.
10 J.-J. Chen, Z.-Y. Huang, T.-S. Liu, M.-D. Tsai and K.-L. Huang, *Appl. Opt.*, 2015, **54**, E146–E152.
11 H. J. Lee, S. An, J. H. Hwang, S.-G. Jung, H. S. Jo, K. N. Kim, Y. S. Shim, C. H. Park, S. S. Yoon and Y. W. Park, *ACS Appl. Mater. Interfaces*, 2014, **7**, 68–74.
12 C. Tang and H. Liu, *Composites, Part A*, 2008, **39**, 1638–1643.
13 E. A. Widder, *Science*, 2010, **328**, 704–708.
14 X. Wang, H. Wang and H. R. Brown, *Soft Matter*, 2011, **7**, 211–219.
15 S. An, C. Lee, M. Liou, H. S. Jo, J.-J. Park, A. L. Yarin and S. S. Yoon, *ACS Appl. Mater. Interfaces*, 2014, **6**, 13657–13666.
16 S. An, H. S. Jo, D. Y. Kim, H. J. Lee, B. K. Ju, S. S. Al-Deyab, J. H. Ahn, Y. Qin, M. T. Swihart, A. L. Yarin and S. S. Yoon, *Adv. Mater.*, 2016, **28**, 7149–7154.
17 M. W. Lee, S. An, C. Lee, M. Liou, A. L. Yarin and S. S. Yoon, *J. Mater. Chem. A*, 2014, **2**, 7045–7053.

18 K. Manabe, S. Nishizawa, K.-H. Kyung and S. Shiratori, *ACS Appl. Mater. Interfaces*, 2014, **6**, 13985–13993.
19 D. Li, Y. Wang and Y. Xia, *Adv. Mater.*, 2004, **16**, 361–366.
20 G. S. Bisht, G. Canton, A. Mirsepassi, L. Kulinsky, S. Oh, D. Dunn-Rankin and M. J. Madou, *Nano Lett.*, 2011, **11**, 1831–1837.
21 S. An, M. W. Lee, H. S. Jo, S. S. Al-Deyab and S. S. Yoon, *J. Aerosol Sci.*, 2016, **95**, 67–72.
22 D. Kim, H.-C. Lee, J. Y. Woo and C.-S. Han, *J. Phys. Chem. C*, 2010, **114**, 5817–5821.
23 D. Jung, D. Kim, K. H. Lee, L. J. Overzet and G. S. Lee, *Sens. Actuators, A*, 2013, **199**, 176–180.
24 D. Kim, L. Zhu, D.-J. Jeong, K. Chun, Y.-Y. Bang, S.-R. Kim, J.-H. Kim and S.-K. Oh, *Carbon*, 2013, **63**, 530–536.
25 T. Kim, Y. W. Kim, H. S. Lee, H. Kim, W. S. Yang and K. S. Suh, *Adv. Funct. Mater.*, 2013, **23**, 1250–1255.
26 S. Sorel, D. Bellet and J. N. Coleman, *ACS Nano*, 2014, **8**, 4805–4814.
27 H.-J. Kim, Y. Kim, J.-H. Jeong, J.-H. Choi, J. Lee and D.-G. Choi, *J. Mater. Chem. A*, 2015, **3**, 16621–16626.